JCI insight

RESEARCH ARTICLE

Fibulin-1c regulates transforming growth factor–β activation in pulmonary tissue fibrosis

Gang Liu,[1,2,3] Marion A. Cooley,[4] Andrew G. Jarnicki,[1,5] Theo Borghuis,[6] Prema M. Nair,[1] Gavin Tjin,[7] Alan C. Hsu,[1] Tatt Jhong Haw,[1] Michael Fricker,[1] Celeste L. Harrison,[1] Bernadette Jones,[1] Nicole G. Hansbro,[1,2,3] Peter A. Wark,[1] Jay C. Horvat,[1] W. Scott Argraves,[8] Brian G. Oliver,[2,7] Darryl A. Knight,[1] Janette K. Burgess,[6,7] and Philip M. Hansbro[1,2,3]

[1]Priority Research Centre for Healthy Lungs, Hunter Medical Research Institute, and the University of Newcastle, Newcastle, New South Wales, Australia. [2]School of Life Sciences, University of Technology Sydney, Sydney, New South Wales, Australia. [3]Centenary Institute, Sydney, New South Wales, Australia. [4]Department of Oral Biology and Diagnostic Sciences, Augusta University, Augusta, Georgia, USA. [5]Department of Pharmacology and Therapeutics, University of Melbourne, Parkville, Victoria, Australia. [6]University of Groningen, University Medical Center Groningen, Groningen Research Institute for Asthma and COPD, Department of Pathology and Medical Biology, Groningen, Netherlands. [7]Woolcock Institute of Medical Research, Discipline of Pharmacology, the University of Sydney, Sydney, New South Wales, Australia. [8]Department of Regenerative Medicine and Cell Biology, Medical University of South Carolina, Charleston, South Carolina, USA.

Tissue remodeling/fibrosis is a major feature of all fibrotic diseases, including idiopathic pulmonary fibrosis (IPF). It is underpinned by accumulating extracellular matrix (ECM) proteins. Fibulin-1c (Fbln1c) is a matricellular ECM protein associated with lung fibrosis in both humans and mice and stabilizes collagen formation. Here we discovered that Fbln1c was increased in the lung tissues of patients with IPF and experimental bleomycin-induced pulmonary fibrosis. *Fbln1c*-deficient (*Fbln1c*$^{-/-}$) mice had reduced pulmonary remodeling/fibrosis and improved lung function after bleomycin challenge. Fbln1c interacted with fibronectin, periostin, and tenascin-C in collagen deposits following bleomycin challenge. In a potentially novel mechanism of fibrosis, Fbln1c bound to latent TGF-β–binding protein 1 (LTBP1) to induce TGF-β activation and mediated downstream Smad3 phosphorylation/signaling. This process increased myofibroblast numbers and collagen deposition. Fbln1c and LTBP1 colocalized in lung tissues from patients with IPF. Thus, Fbln1c may be a novel driver of TGF-β–induced fibrosis involving LTBP1 and may be an upstream therapeutic target.

Introduction

Tissue remodeling and fibrosis are major features of fibrotic diseases, including those affecting the lung, such as idiopathic pulmonary fibrosis (IPF) (1, 2). Fibrosis results from the excessive tissue deposition of extracellular matrix (ECM) proteins produced predominantly from myofibroblasts, which leads to increased collagen deposition in tissues (3). Multiple ECM proteins are involved in fibrosis, including collagens, fibronectin (Fn), periostin (Postn), and tenascin-C (Tnc) (3–5). The mechanisms that drive fibrosis involve TGF-β–mediated pathways (6), but how these are induced remains incompletely understood.

IPF is a chronic, progressive, and lethal interstitial fibrotic lung disease that occurs primarily in older adults (7). Its prognosis is poor, with an average survival of 2–3 years after diagnosis, shorter than most cancers (7, 8). IPF is characterized by dyspnea, dry cough, and progressive airway and lung tissue remodeling (9). Patients with IPF have increased collagen deposition around the small airways (10) and interstitial and airspace fibrosis of the lung parenchyma (11). This leads to reduced lung function, including a decline in forced vital capacity that accompanies disease progression (12). The cause of IPF is unknown; however, cigarette smoke, environmental insults, and genetic predisposition are primary etiological factors (13, 14), and TGF-β–mediated pathways and downstream Smad signal transducers are well known to be involved (6). Current therapies directly target the tissue remodeling in IPF but have limited efficacy. Nintedanib targets multiple receptors and tyrosine kinases

Authorship note: WSA is deceased.

Conflict of interest: The authors have declared that no conflict of interest exists.

Submitted: August 28, 2018
Accepted: July 16, 2019
Published: July 25, 2019.

Reference information: *JCI Insight*. 2019;4(16):e124529. https://doi.org/10.1172/jci.insight.124529.

Table 1. Human subject history

Donor	Sex	Age	Diagnosis	Smoking history
Non-IPF control 1	Male	30	Resection for thoracic malignancy	None
Non-IPF control 2	Female	62	Resection for thoracic malignancy	Ex-smoker
Non-IPF control 3	Male	47	MVA	None
Non-IPF control 4	Male	60	Emphysema	Ex-smoker
Non-IPF control 5	Female	62	Resection for thoracic malignancy	Ex-smoker
Non-IPF control 6	Male	19	MVA	None
Non-IPF control 7	Male	52	Healthy – hemorrhage	None
Non-IPF control 8	Female	62	Emphysema	None
IPF 1	Female		IPF	None
IPF 2	Male	52	IPF	None
IPF 3	Male	57	IPF	Ex-smoker
IPF 4	Male	55	IPF	Ex-smoker
IPF 5	Female	58	IPF	None
IPF 6	Male	58	IPF	Ex-smoker
IPF 7	Male	58	IPF	None

All patients with IPF had end-stage disease and had lung transplantation. MVA, motor vehicle accident.

and slows disease progression in patients with IPF (15). Pirfenidone, an antifibrotic drug, downregulates the production of TGF-β and suppresses the progression of pulmonary fibrosis (6). Both drugs delay the impairment of lung function and improve the survival rate of patients with IPF (6, 15). However, these treatments are not cures, often have debilitating side effects, and delay rather than inhibit or reverse pulmonary remodeling.

Fibulin-1 (Fbln1), a secreted glycoprotein, is an important matricellular ECM protein (16). It facilitates the stabilization and binding of other ECM proteins, such as Fn, Postn, Tnc, and versican during collagen deposition (1). There are 4 Fbln1 variants (Fbln1a, -b, -c, and -d) in humans that differ in their C-terminal sequences, but only Fbln1c and -d occur in mice (17). Fbln1c is the variant that is associated with respiratory diseases in humans and mice (1, 18). We previously showed that Fbln1 protein levels are increased in serum/plasma and lung tissue from patients with IPF (18); however, the level of the Fbln1c variant was not assessed. We also showed that a Fbln1c peptide increases the proliferation of lung fibroblasts from patients with IPF (19) and that *Fbln1c*-deficient (*Fbln1c*$^{-/-}$) mice are protected against bleomycin-induced small airway remodeling (1). We also showed similar roles for Fbln1c in fibrosis in chronic obstructive pulmonary disease (COPD) and asthma (1, 20). However, the roles of Fbln1c in pulmonary fibrosis and the mechanisms involved remain unknown.

In this study, we show that Fbln1c levels are increased in the lung tissues of patients with IPF and demonstrate that Fbln1c is essential for the development of an experimental model of pulmonary fibrosis. Inhibition of *Fbln1c* in mice protects them from developing airway and lung remodeling/fibrosis through the attenuation of the TGF-β signaling pathway and myofibroblast generation. We identify a potentially novel mechanism that involves Fbln1c binding to latent TGF-β–binding protein 1 (LTBP1) to activate the TGF-β signaling pathway to induce fibrosis. These data increase fundamental understanding of development of fibrosis, and Fbln1c may drive TGF-β activation and signaling and be a potential upstream therapeutic target in IPF and other fibrotic diseases.

Results

Fbln1 levels are increased in the lung tissues of patients with IPF. To understand the role of Fbln1c in fibrosis, we used IPF, one of severe fibrotic diseases (9), as an example. Lung tissues were obtained from patients with IPF and controls with normal lungs (Table 1). Fbln1c protein levels, measured by immunohistochemistry, were significantly increased specifically in fibrotic areas of the lungs from patients with IPF but not in nonfibrotic areas or in the lungs from controls (Figure 1A).

Fbln1c is increased around small airways and in lungs in experimental bleomycin-induced pulmonary fibrosis. To determine the role of Fbln1c in pulmonary fibrosis, a previously described experimental model of bleomycin-induced lung fibrosis was used (21–23). One dose of bleomycin was administered (0.05 U, intranasally), and collagen deposition around the small airways and in lungs was assessed after 7, 14, 21, and

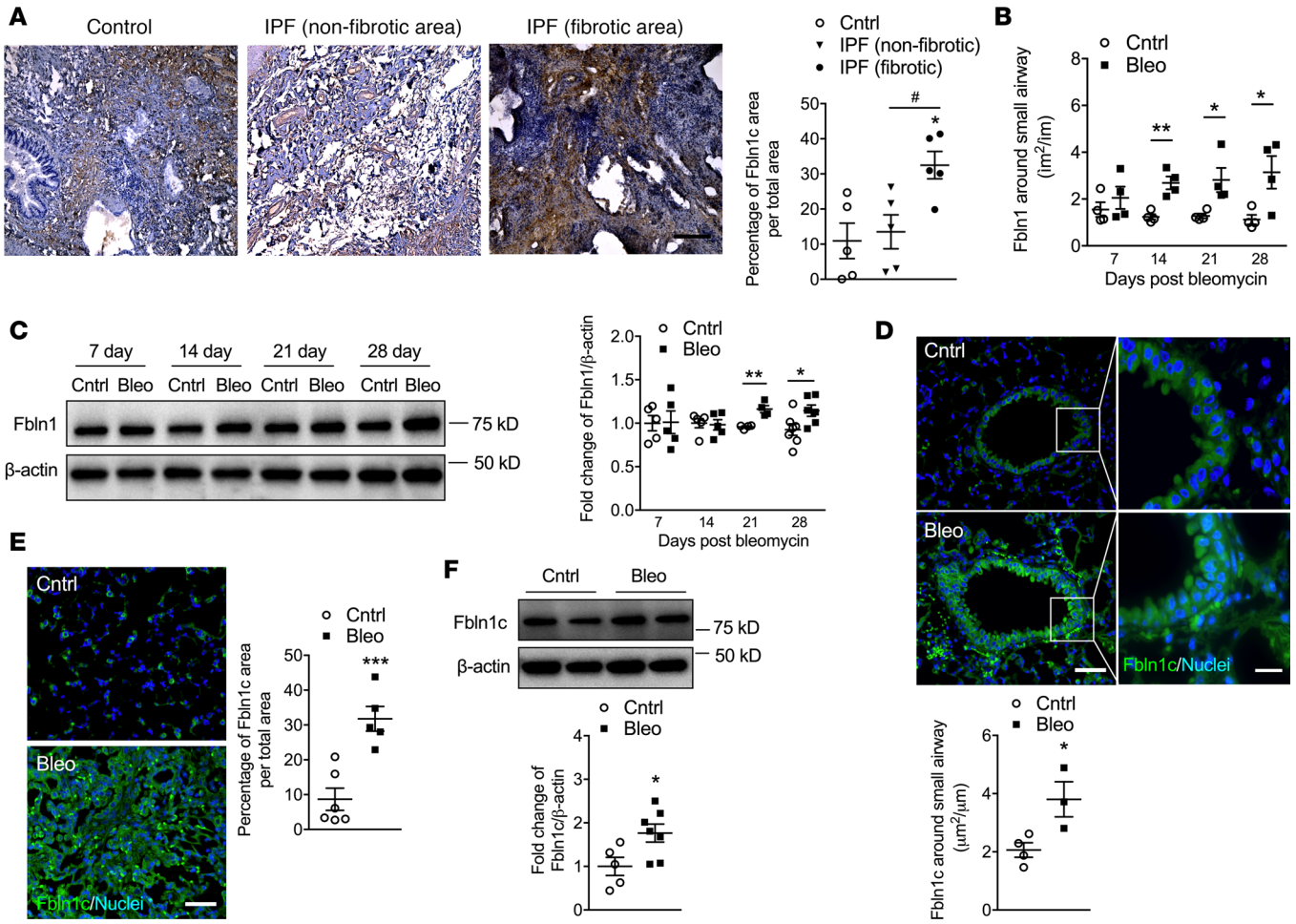

Figure 1. Fbln1c is increased in patients with IPF and bleomycin-induced experimental pulmonary fibrosis. (**A**) Fbln1c deposition in lung sections from the nonfibrotic area and fibrotic area in patients with IPF and from healthy lung controls stained using immunohistochemistry (left); scale bar: 200 μm. Fbln1c-stained areas were quantified with normalization to the total area (right, n = 7–8). A single bleomycin challenge was used to induce pulmonary fibrosis in WT and *Fbln1c*$^{-/-}$ mice. Controls were challenged with PBS. $^{\#}P < 0.05$, compared to nonfibrotic IPF. (**B**) Stained areas of total Fbln1 were quantified around small airways with normalization to the perimeter of the basement membrane (Pbm) (n = 6–8). (**C**) Fbln1 protein levels were assessed using immunoblot of whole lung tissues (left), and fold change of densitometry was normalized to β-actin and quantified (right, n = 8). (**D**) Twenty-eight days after bleomycin or PBS challenge, lung sections were assessed for protein of the 1c isoform, Fbln1c, around small airways using immunofluorescence (top); scale bar: 50 μm. (Insets show expanded images of indicated regions; scale bar: 15 μm.) Fbln1c-stained areas around airways were quantified with normalization to the Pbm (bottom, n = 8). (**E**) Fbln1c protein area in parenchyma was determined using immunofluorescence (left); scale bar: 50 μm. Fbln1c-stained areas were quantified with normalization to total area (right, n = 8). (**F**) Fbln1c protein levels were assessed in whole lungs using immunoblot (top), and fold change of densitometry was quantified with normalization to β-actin (bottom, n = 8). Statistical differences were determined with 2-tailed Student's t test. $^{*}P < 0.05$, $^{**}P < 0.01$, and $^{***}P < 0.001$ compared with human healthy lung controls or PBS-challenged mouse controls.

28 days. Bleomycin challenge induced significant deposition of collagen around the small airways after 21 days, which increased further after 28 days, compared with sham-challenged controls (Figure 1B and Supplemental Figure 1; supplemental material available online with this article; https://doi.org/10.1172/jci.insight.124529DS1). Concomitant with this, there were significant increases in the levels of total lung hydroxyproline, a surrogate marker for elevated total collagen levels, following bleomycin challenge, in whole lung tissues after 28 days (Supplemental Figure 1).

We then measured Fbln1 protein levels around the airways and in whole lung tissues over the 28-day time course after bleomycin challenge using immunohistochemistry. Fbln1 deposition around the small airways was significantly increased from 14 days, compared with sham-challenged controls (Figure 1B and Supplemental Figure 2). Fbln1 protein levels in whole lung tissues assessed using immunoblotting were also significantly increased following bleomycin exposure after 21 and 28 days (Figure 1C).

Lung fibrosis was maximally increased around the airways and in the lungs after 28 days; thus, we measured Fbln1c-specific protein levels in mouse lung sections at this time point. Deposition of Fbln1c was

significantly increased around the small airways (Figure 1D) and in the parenchyma (Figure 1E) 28 days after bleomycin challenge, and the Fbln1c protein levels were also increased in whole lung tissue (Figure 1F). The increased levels of Fbln1 and Fbln1c in mice treated with 28 days of bleomycin challenge are similar, indicating that Fbln1c plays key roles in lung fibrosis compared with Fbln1d.

Genetic deletion of Fbln1c protects against experimental bleomycin-induced pulmonary fibrosis. The 28-day time point after bleomycin treatment was also used to assess the effect of Fbln1c deficiency. Deletion of all *Fbln1* isoforms in mice is embryonically lethal; thus, *Fbln1c*$^{-/-}$ mice were created and used (1). *Fbln1c* mRNA levels were significantly increased in wild-type (WT) mouse lungs 28 days after bleomycin challenge but were undetectable in *Fbln1c*$^{-/-}$ mice (Figure 2A). However, *Fbln1d* mRNA levels in WT and *Fbln1c*$^{-/-}$ mice were not altered (Figure 2B). The absence of *Fbln1c* completely inhibited the development of bleomycin-induced collagen deposition around the small airways compared with WT mice (Figure 2C), congruent with our previous findings in COPD (1). In addition, *Fbln1c* deficiency completely prevented increases in total and soluble collagen levels (Figure 2D) and in type I collagen α1 (Col1a1), the most abundant collagen in diseased lungs, in whole lung tissues (Figure 2, E and F).

Second harmonic generation (SHG) microscopy has been recently used as a powerful and robust tool to visualize changes in collagen microstructure in tissues (24, 25). SHG emits 2-photon scattering in the focal volume, forward (F_{SHG}) and backward (B_{SHG}), and the F_{SHG}/B_{SHG} relationship is sensitive to the spatial extent of SHG-generated scattering to indicate the disorder of arrangement and density of collagen fibrils. The ratio of the F_{SHG}/B_{SHG} area was significantly increased in WT mice 28 days after bleomycin challenge compared with controls (Figure 2G and Supplemental Figure 3). Again, *Fbln1c*$^{-/-}$ mice were protected against this increase.

The balance of matrix metalloproteinase (MMP) and tissue inhibitor of metalloproteinase (TIMP) regulates ECM protein production (1). Thus, we then measured the mRNA levels of these proteins in the lungs from WT and *Fbln1c*$^{-/-}$ mice. Bleomycin-challenged WT mice had substantial increases in the mRNA levels of *Mmp1*, *-3*, *-8*, *-12*, and *-13* in lung tissues after 28 days compared with controls (Supplemental Figure 4, A–E). These increases were abrogated in *Fbln1c*$^{-/-}$ mice. The mRNA levels of *Timp1* were also increased in bleomycin-challenged WT mice but not *Fbln1c*$^{-/-}$ mice (Supplemental Figure 4F).

To determine whether protection against pathological changes in *Fbln1c*$^{-/-}$ mice prevented functional changes, lung function parameters were assessed in WT and *Fbln1c*$^{-/-}$ mice 28 days after bleomycin challenge. Bleomycin challenge increased tissue damping and tissue elastance and reduced lung compliance in WT mice, but *Fbln1c*$^{-/-}$ mice were protected against these changes (Figure 2, H–J).

Fbln1c deficiency protects against bleomycin-induced accumulation of Fn and Tnc around the small airways and in whole lung tissues. Fbln1 is critical for ECM stabilization (1); thus, we next assessed the specific role of Fbln1c in the deposition of ECM and remodeling around the small airways in bleomycin-induced pulmonary fibrosis. Bleomycin challenge induced Fn and Tnc deposition in the basement membrane around the small airways after 28 days in WT mice (Figure 3, A and B). Again, *Fbln1c*$^{-/-}$ mice were protected against these changes. In contrast, Postn deposition was not altered in WT or *Fbln1c*$^{-/-}$ mice (Figure 3C).

We then assessed the role of Fbln1c in ECM protein deposition in whole lung tissues. Bleomycin challenge substantially increased *Fn* and *Tnc* mRNA levels in WT mouse lungs, whereas *Fbln1c*$^{-/-}$ mice were protected (Figure 3, D and E). *Postn* mRNA levels in lungs were not altered in WT or *Fbln1c*$^{-/-}$ mice after bleomycin challenge (Figure 3F). Bleomycin challenge resulted in increased Fn protein levels in the lungs from WT mice compared with controls, whereas Tnc (either variant) and Postn levels were not altered (Figure 3G). The levels of all of these proteins were significantly reduced in bleomycin-challenged *Fbln1c*$^{-/-}$ mice compared with WT controls. Tnc and Postn levels were significantly reduced even compared with controls not treated with bleomycin. We also measured the deposition of other ECM components, versican and ECM1, but found no significant differences between bleomcyin-challenged WT and *Fbln1c*$^{-/-}$ mice compared to controls (not shown).

Fbln1c binds with LTBP1 to activate TGF-β. To investigate the mechanisms involved in Fbln1c-regulated pulmonary fibrosis, we measured the levels of TGF-β, its activation, and its regulation in the lungs of bleomycin-challenged mice. The mRNA levels of *Tgfb* were increased in the lung tissues of bleomycin-challenged WT and *Fbln1c*$^{-/-}$ mice (Figure 4A). The levels of active TGF-β_1 proteins measured by ELISA were increased in WT mice; however, levels of active TGF-β_1 did not increase in *Fbln1c*$^{-/-}$ mice (Figure 4B). LTBP1 regulates TGF-β_1 activation, and its levels were increased in both WT and *Fbln1c*$^{-/-}$ mice after bleomycin challenge, with no significant differences between them (Figure

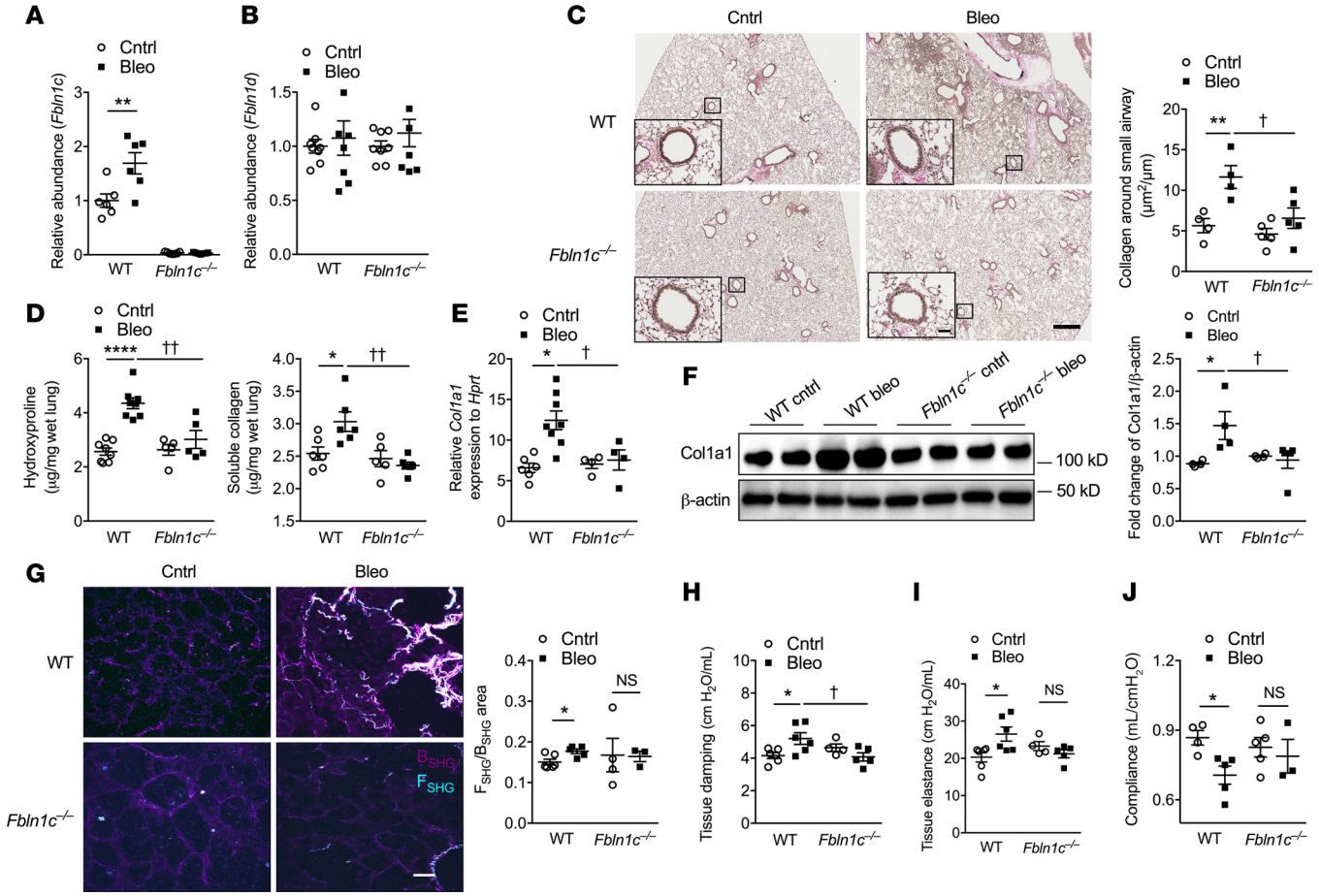

Figure 2. Bleomycin challenge of *Fbln1c*$^{-/-}$ mice does not induce airway or lung fibrosis or impair lung function. A single bleomycin challenge was used to induce pulmonary fibrosis in WT and *Fbln1c*$^{-/-}$ mice that were assessed 28 days later. Controls received PBS. (**A**) *Fbln1c* and (**B**) *Fbln1d* mRNA levels in whole lungs determined using quantitative real-time PCR (qRT-PCR) (n = 6–8). (**C**) Lung sections were stained with Verhoeff-Van Gieson stain (left, scale bar: 500 μm; insets show expanded images of indicated regions; scale bar: 50 μm) and areas of collagen around small airways quantified with normalization to the Pbm (right, n = 8). (**D**) Total collagen levels were assessed by measuring hydroxyproline (left) and soluble collagen (right) in the whole lung tissues (n = 8). (**E**) Type I collagen (*Col1a1*) mRNA levels were measured in whole lungs using qRT-PCR (n = 8). (**F**) Col1a1 protein levels were measured in whole lungs using immunoblot (left), and fold change was quantified with normalization to β-actin (right, n = 8). (**G**) Collagen fibers were detected by second harmonic generation (SHG) microscopy (left), and fiber areas were calculated by forward (F_{SHG})/backward (B_{SHG}) SHG ratios (right, n = 4–6; scale bar: 100 μm). Lung function in terms of (**H**) tissue damping, (**I**) tissue elastance, and (**J**) lung compliance was measured using invasive plethysmography and the forced oscillation technique (n = 5–8). Statistical differences were determined with 1-way ANOVA followed by Bonferroni's posttest. *P < 0.05, **P < 0.01, and ****P < 0.0001 compared with PBS-challenged WT or *Fbln1c*$^{-/-}$ controls. $^{\dagger}P$ < 0.05, and $^{\dagger\dagger}P$ < 0.01 compared with bleomycin-challenged WT controls. NS, not significant.

4C). We then measured the downstream molecules in the TGF-β signaling pathway, Smad2, Smad3, and Smad4. Bleomycin challenge significantly reduced *Smad3* mRNA levels (Supplemental Figure 5A) but increased phosphorylated Smad3 (p-Smad3) protein levels in the lungs of WT but not *Fbln1c*$^{-/-}$ mice (Figure 4D). In contrast, the mRNA levels of *Smad2* and *Smad4* in the lungs of WT and *Fbln1c*$^{-/-}$ mice were not altered (Supplemental Figure 5, B and C).

To further assess mechanisms, we immunoprecipitated Fbln1c and identified its binding relationship with LTBP1. LTBP1s were detectable when immunoprecipitated with Fbln1c from naive WT mouse lung lysates assessed using immunoblot (Figure 4E). This did not occur in proteins from *Fbln1c*$^{-/-}$ mice. This confirmed that a binding interaction exists between Fbln1c and LTBP1.

Collectively these data show that the absence of Fbln1c does not affect LTBP1 levels but that Fbln1c is required for the activation of TGF-β_1 and downstream Smad3 phosphorylation.

Fbln1c regulates fibroblast activation and conversion into myofibroblasts and collagen deposition. To further investigate the role of Fbln1c in the mechanisms of pathogenesis of fibrosis, primary lung fibroblasts were isolated from WT and *Fbln1c*$^{-/-}$ mice and stimulated with recombinant TGF-β_1 protein. As we stimulated fibroblasts with recombinant TGF-β_1 protein, we could not distinguish between TGF-β_1 protein that was

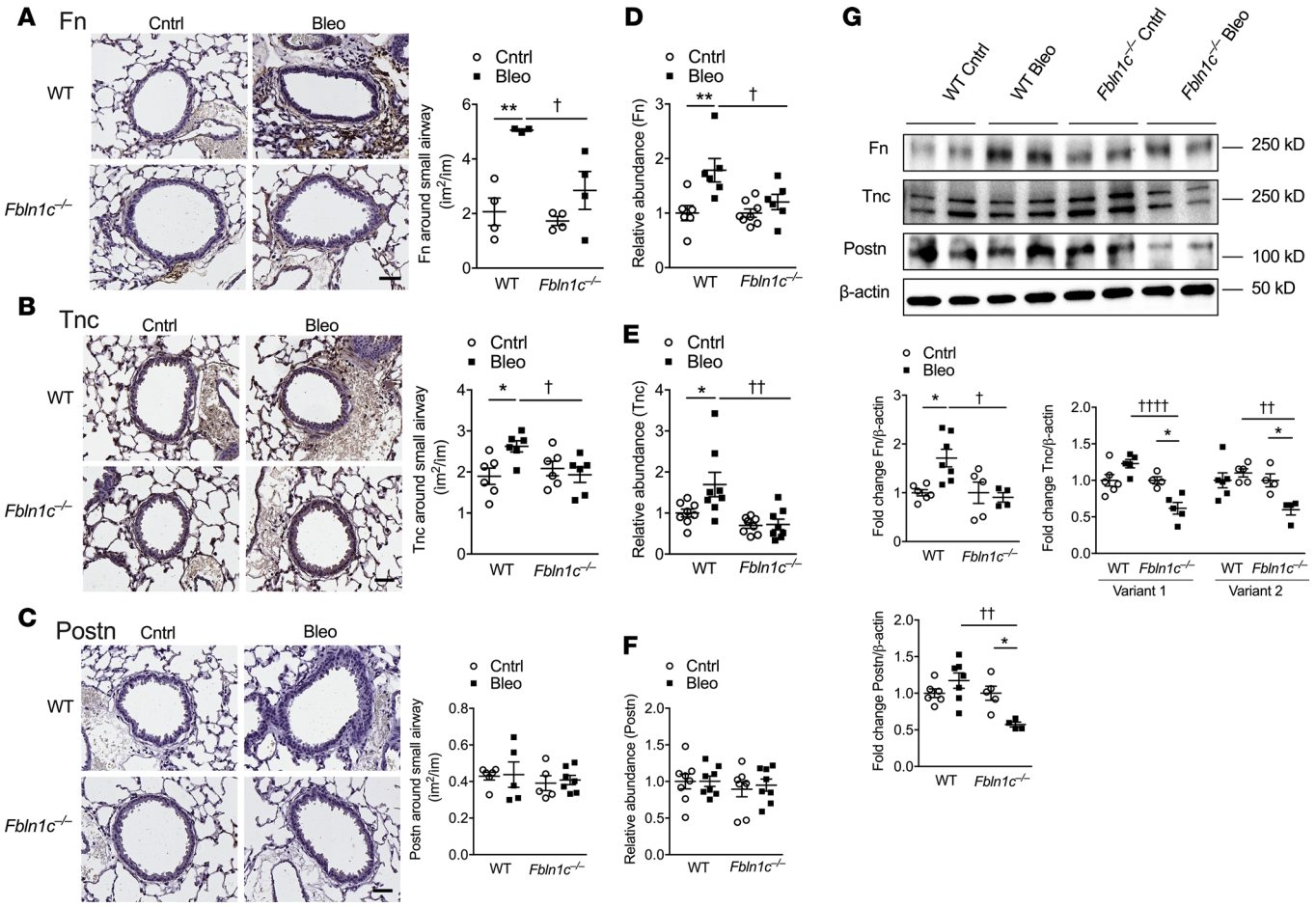

Figure 3. Bleomycin challenge in *Fbln1c*$^{-/-}$ mice does not increase the levels of ECM proteins around the small airway or in whole lung tissue. A single bleomycin challenge was used to induce pulmonary fibrosis in WT and *Fbln1c*$^{-/-}$ mice that were assessed 28 days later. Controls received PBS. (**A**) Fibronectin (Fn), (**B**) tenascin-C (Tnc), and (**C**) periostin (Postn) deposition in the basement membrane around small airways was assessed using immunohistochemistry and stained areas quantified with normalization to the Pbm (n = 24–40 airways from n = 4–8 mice per group). (**D**) *Fn*, (**E**) *Tnc*, and (**F**) *Postn* mRNA levels in lungs were determined using qRT-PCR (n = 6–8). (**G**) Fn, Tnc (variants 1 and 2), and Postn protein levels in whole lung tissues were assessed using immunoblot (top), and fold change was quantified using densitometry with normalization to β-actin (bottom, n = 5–8). Statistical differences were determined with 1-way ANOVA followed by Bonferroni's posttest. $^{*}P < 0.05$, and $^{**}P < 0.01$ compared with PBS-challenged WT controls. $^{\dagger}P < 0.05$, $^{\dagger\dagger}P < 0.01$, and $^{\dagger\dagger\dagger\dagger}P < 0.0001$ compared with bleomycin-challenged WT controls.

administered versus secreted. Thus, we measured *Tgfb* mRNA levels. *Tgfb* mRNA (Figure 5A) and LTBP1 (Figure 5B) levels were increased in lung fibroblasts from both WT and *Fbln1c*$^{-/-}$ mice after stimulation. Thus, the levels of *Tgfb* mRNA and LTBP1 were again unchanged in fibroblasts. Downstream p-Smad3 protein levels were also increased in WT but again not in *Fbln1c*$^{-/-}$ fibroblasts after stimulation (Figure 5C).

TGF-β–stimulated fibroblasts from WT mice developed into myofibroblasts, as indicated by the presence of α–smooth muscle actin (α-SMA), but this was significantly reduced in *Fbln1c*$^{-/-}$ mice (Figure 5D). TGF-β–stimulated fibroblasts from WT mice had significantly increased *Col1a1* mRNA (Figure 5E) and protein (Figure 5F) levels, but these were reduced and completely inhibited, respectively, in *Fbln1c*$^{-/-}$ fibroblasts.

To further explore the role of Fbln1c in the TGF-β signaling pathway, we isolated primary fibroblasts from WT mouse lungs and treated them with BALF (20 μL per mouse from 6 mice pooled to a total of 120 μL) from WT or *Fbln1c*$^{-/-}$ mice 28 days after bleomycin challenge or from controls, for 24 and 48 hours. However, fibroblasts from *Fbln1c*$^{-/-}$ but not WT mice were detached and dead at these time points. We therefore isolated fibroblasts at an earlier time point (6 hours) and lysates were collected. Smad2, -3, and -4 gene expression were largely unaltered in fibroblasts cultured with BALF from WT and *Fbln1c*$^{-/-}$ mice (Supplemental Figure 5, D–F). Col1a1 protein levels were also not changed in fibroblasts incubated with BALF from bleomycin-challenged compared to control WT mice. However, Col1a1 and p-Smad3 proteins were reduced in cells treated with BALF from *Fbln1c*$^{-/-}$ compared with WT mice (Figure 5, G and H).

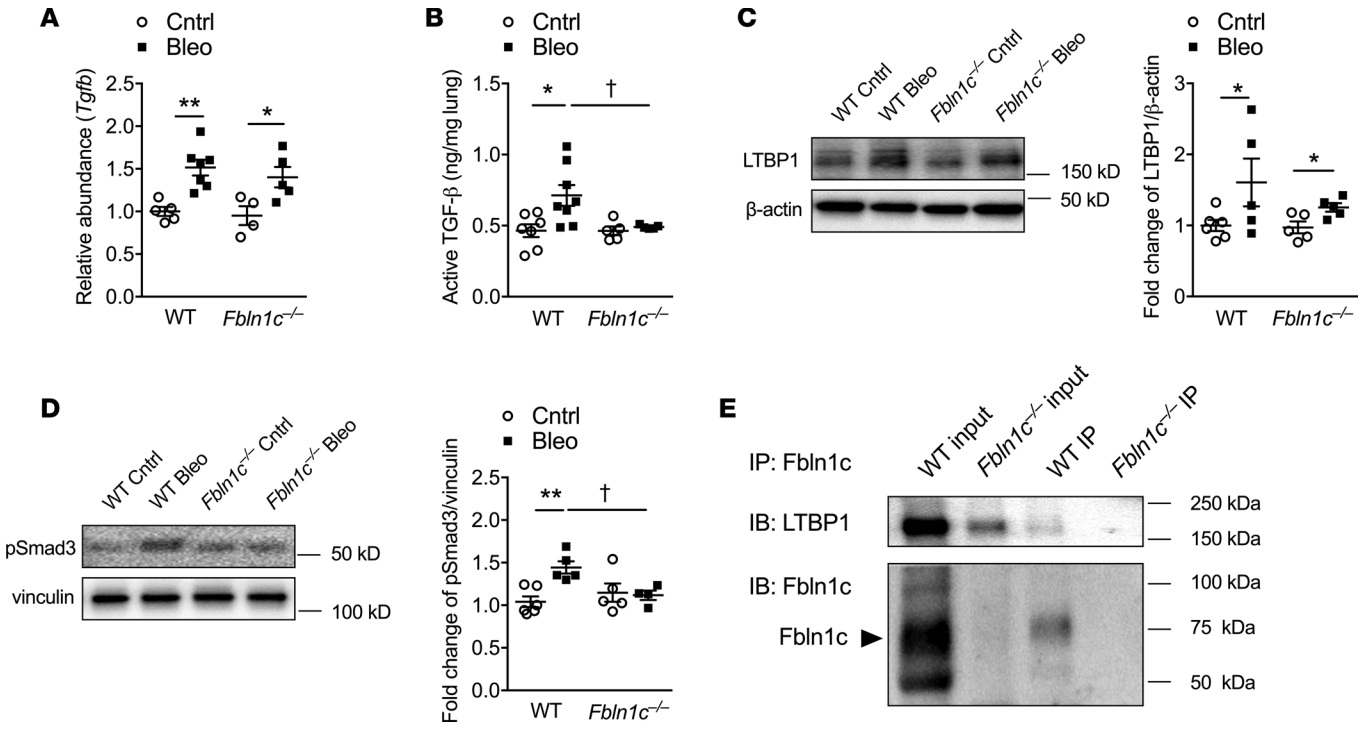

Figure 4. Fbln1c binds with LTBP1 to induce TGF-β activation. A single bleomycin challenge was used to induce pulmonary fibrosis in WT and *Fbln1c*$^{-/-}$ mice that were assessed 28 days later. Controls received PBS. TGF-β (**A**) mRNA and (**B**) active protein levels in whole lung tissues measured using qRT-PCR and ELISA (n = 4–8). (**C**) LTBP1 levels in lungs measured using immunoblot (left) and fold change quantification using densitometry with normalization to β-actin (right, n = 5–8). (**D**) p-Smad3 protein levels in lungs measured using immunoblot (left) and fold change quantified using densitometry with normalization to vinculin (right, n = 5–8). (**E**) Immunoprecipitation (IP) of Fbln1c protein from whole lung tissues and detection of Fbln1c and LTBP1 binding using immunoblot (IB). IB analysis of lung tissues before (input) and after IP. Statistical differences were determined with 1-way ANOVA followed by Bonferroni's posttest. *P < 0.05, and **P < 0.01 compared with PBS-challenged WT controls. †P < 0.05 compared with bleomycin-challenged WT controls.

Fbln1 colocalized with LTBP1 in lungs from patients with IPF. We show that Fbln1c binds to LTBP1 (Figure 4E) to regulate TGF-β activation (Figure 4B) in mouse lungs. To further support this binding relationship in humans, we stained lung sections from patients with IPF and controls with Fbln1 and LTBP1 and assessed their colocalization. We detected Fbln1 here because of lack of a specific antibody to distinguish human Fbln1c by immunofluorescence. Fbln1 and LTBP1 protein colocalized in lung sections from patients with IPF but not controls without IPF (Figure 6).

Discussion

Aberrant deposition of ECM proteins and fibrosis have severe pathological consequences in many diseases, including in the respiratory tract, but no effective treatments currently exist. Here we identify a critical role for the ECM protein Fbln1c in regulating airway and lung remodeling during the pathogenesis of pulmonary fibrosis. For the first time to our knowledge, we showed specific increases in Fbln1c protein levels in the lungs of patients with IPF. Increased collagen and Fbln1c deposition were also observed around the airways and in the lung tissues in experimental bleomycin-induced pulmonary fibrosis. Genetic inhibition of *Fbln1c* prevented increases in bleomycin-induced collagen around the airways and in the lungs, inhibited MMP expression, and also protected against the impairment of lung function. Fbln1c also bound to Fn and Tnc, and these ECM proteins and Postn were reduced with genetic inhibition. We discovered a potentially novel profibrotic mechanism whereby Fbln1c bound to LTBP1 to induce TGF-β activation of the downstream Smad3 pathway and collagen deposition, as well as the conversion of fibroblasts to myofibroblasts (Figure 7). We validated these experimental links by showing that Fbln1c colocalized with LTBP1 in the lung tissues of patients with IPF.

Several experimental models are available to examine lung fibrosis, all of which have limitations. We employed the widely used bleomycin-induced mouse model of pulmonary fibrosis to show that Fbln1c is increased around the airways and lungs. The concern with this model is that the bleomycin-induced fibrosis is partially reversible, unlike human lung fibrosis (26). However, it does develop histological alterations sim-

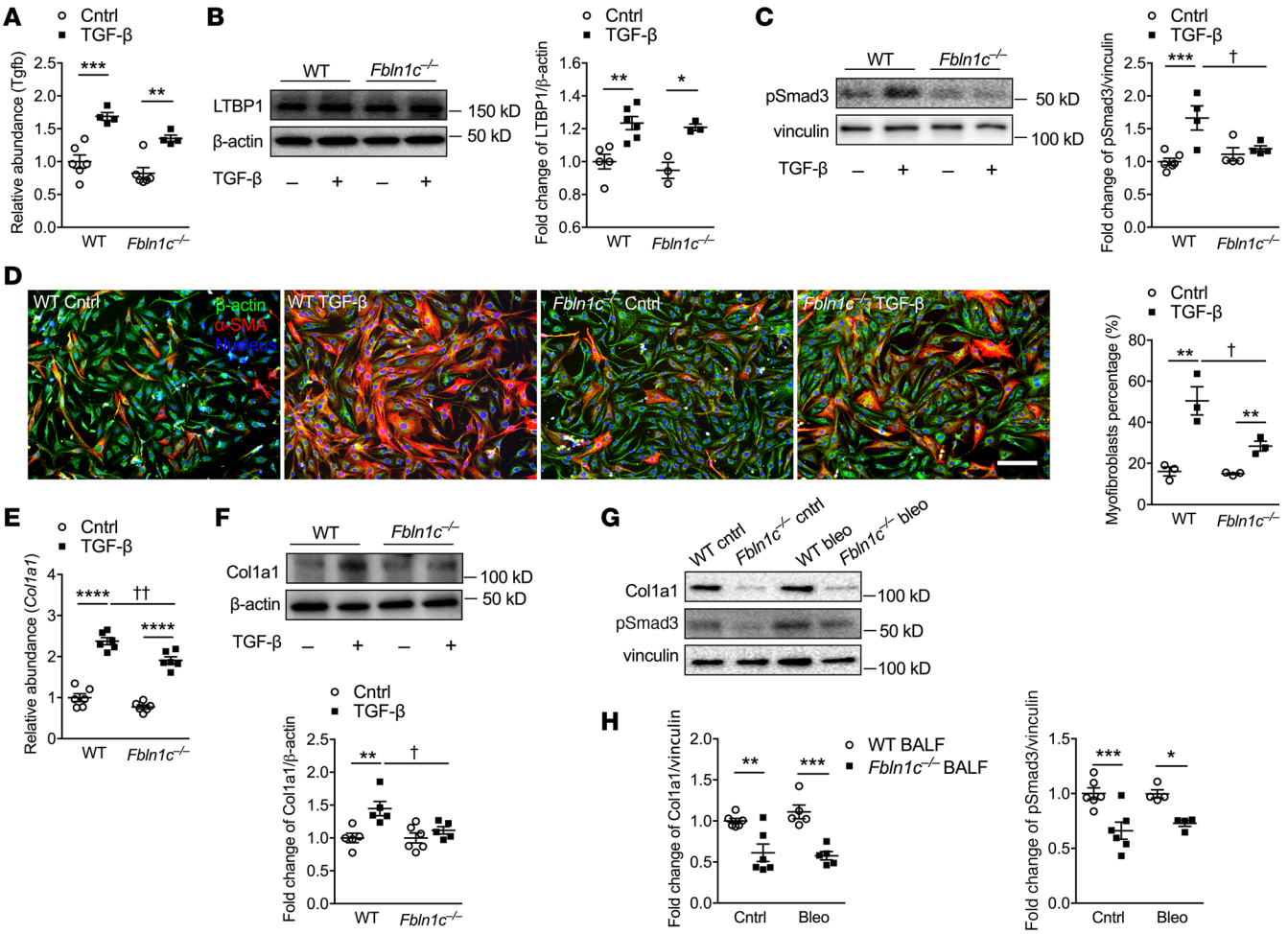

Figure 5. Fbln1c binds to LTBP1 to activate TGF-β and induce fibroblast activation and collagen deposition. A single bleomycin challenge was used to induce pulmonary fibrosis in WT and *Fbln1c*$^{-/-}$ mice that were assessed 28 days later. Controls received PBS. (**A**) *Tgfb* mRNA levels in lungs were measured using qRT-PCR (n = 6). (**B**) LTBP1 levels in whole lung tissues were measured using immunoblot (left), and fold change was quantified using densitometry with normalization to β-actin (right, n = 6). Primary lung fibroblasts were isolated from whole lung tissues of naive WT and *Fbln1c*$^{-/-}$ mice and stimulated with TGF-β or control medium. (**C**) p-Smad3 protein levels in fibroblast lysates were measured using immunoblot (left), and fold change was quantified using densitometry with normalization to vinculin (right, n = 6). (**D**) Fibroblasts were stained with β-actin, and myofibroblasts were stained with α-SMA (left), and the percentage of myofibroblasts as a percentage of total fibroblasts was determined (right; scale bar: 500 μm; n = 6). (**E**) *Col1a1* mRNA levels in fibroblast lysates were measured using qRT-PCR (n = 6). (**F**) Col1a1 protein levels in fibroblast lysates were measured using immunoblot, and fold change was quantified using densitometry with normalization to β-actin (right, n = 6). Primary mouse lung fibroblasts from WT mice were incubated with bronchoalveolar lavage fluid (BALF, 20 μL each mouse, 120 μL total) from WT and *Fbln1c*$^{-/-}$ mice after 28 days of bleomycin challenge and PBS controls for 6 hours. (**G**) Col1a1 and p-Smad3 protein in fibroblast lysates were measured using immunoblot, and (**H**) fold change was quantified using densitometry with normalization to vinculin (right, n = 6). Statistical differences were determined with 1-way ANOVA followed by Bonferroni's posttest. $^{*}P < 0.05$, $^{**}P < 0.01$, $^{***}P < 0.001$, and $^{****}P < 0.0001$ compared with WT fibroblast controls. $^{\dagger}P < 0.05$, and $^{\dagger\dagger}P < 0.01$ compared with TGF-β–stimulated WT fibroblast controls.

ilar to those observed in patients with IPF, and the use of this model and analysis of transgenic mice have greatly advanced our understanding of the disease (26).

Through its interaction with multiple ECM proteins, Fbln1c was revealed to play a major role in directing ECM deposition in pulmonary fibrosis. *Fbln1c*$^{-/-}$ mice were completely protected against collagen deposition around the small airways and in whole lung tissues. Type I collagen is the most abundant ECM protein in the lung that constitutes the majority of the matrix structure. Collagen production can be regulated by fibroblast activation, inflammation, alterations in the balance of enzymes that cleave and promote fiber assembly, and cross-linking and stability of the ECM. Fbln1 is known to bind many other ECM proteins to stabilize the structure (27).

MMPs, particularly MMP1, -8, and -13, are prevalent proteases that degrade ECM proteins in the lung. MMP1 (protein) and MMP3 (protein and mRNA) levels are increased in the lungs of patients with IPF, and *Mmp3*$^{-/-}$ mice are protected against bleomcyin-induced lung fibrosis (28). MMP8 protein levels

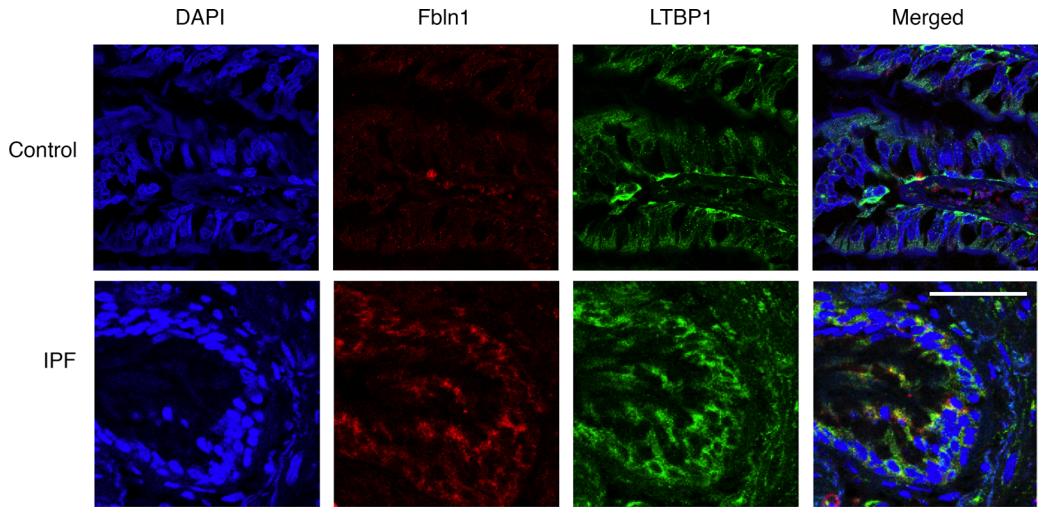

Figure 6. Fbln1 and LTBP1 colocalize in IPF patient lungs. Lung sections were obtained from patients with IPF and controls. Fbln1 (shown in red) and LTBP1 (shown in green) were stained using immunofluorescence, and nuclei were stained with DAPI (shown in blue). Scale bar: 50 μm.

are also increased in the BALF from patients with IPF and in the lungs of mice with bleomcyin-induced pulmonary fibrosis (29). We also found that MMPs were significantly increased in WT mouse lungs after bleomycin challenge. MMP activity is counterbalanced by the inhibitory activity of TIMPs (30); accordingly, we showed *Timp1* mRNA expression was also increased in WT mouse lungs after bleomcyin challenge. Notably, the aberrant levels of MMPs and *Timp1* were not observed in *Fbln1c*$^{-/-}$ mice, identifying a potential role for Fbln1c in regulating MMP/TIMP activity in pulmonary fibrosis. MMPs are known to be able to limit the extent of fibrosis and may be induced to control remodeling. Thus, in the absence of Fibln1c and fibrosis, MMP responses are not needed. It remains unknown how Fbln1c regulates MMPs and TIMPs and whether the effects are direct or indirect, which requires further study.

Few studies have examined alterations in lung function in the bleomycin model, but we demonstrated the impairment of tissue damping, tissue elastance, and lung compliance, which are relevant to IPF physiology (31). Tissue damping is a measure of whole lung tissue resistance, while tissue elastance and compliance indicate the level of lung stiffness (32). Our lung function study results demonstrate that the lungs of bleomycin-challenged WT mice stiffen because of fibrosis, as occurs in patients with IPF (33, 34). However, these lung function changes do not develop in the absence of *Fbln1c*, indicating its critical role in pulmonary fibrosis. Deletion of total *Fbln1* in mice results in perinatal lethality, but *Fbln1c*$^{-/-}$ mice develop a normal phenotype (1). Thus, therapeutically targeting Fbln1c, rather than total Fbln1, may limit adverse effects resulting from the total disruption of Fbln1's role in tissue homeostasis.

Other ECM proteins are also involved in the pathogenesis of IPF. Lung fibroblasts from patients with IPF secrete more Fn and have the capacity to increase Tnc synthesis compared with those from healthy controls (35). We showed that Fn and Tnc deposition increased around small airways after bleomycin challenge of WT mice and that Fbln1c was necessary for these increases. Furthermore, Fn, Tnc, and Postn protein levels in whole lung tissues were reduced in bleomycin-challenged *Fbln1c*$^{-/-}$ mice compared with WT controls. The ECM proteins Fn and Tnc were selected because of their known interactions with Fbln1 (1), while Postn was chosen for its indirect binding to Fbln1 and its effects on collagen deposition (36). It is likely that other ECM proteins are involved in the regulation of matrix deposition. For example, versican affects the early stage of repair processes in IPF (37); however, its protein levels were not changed in lungs between WT and *Fbln1c*$^{-/-}$ mice (data not shown). The protein levels of elastin are increased in fibrotic lung tissue in patients with IPF (38), and many other ECM proteins may also be involved (39). However, a complete characterization of the complex interactions that contribute to the generation of aberrant ECM deposition is beyond the scope of a single study. Levels of ECM proteins may also be affected by changes in other factors that control their transcription, such as microRNAs, which have also been shown to be dysregulated in IPF (2), and other chronic fibrosis–associated diseases (40).

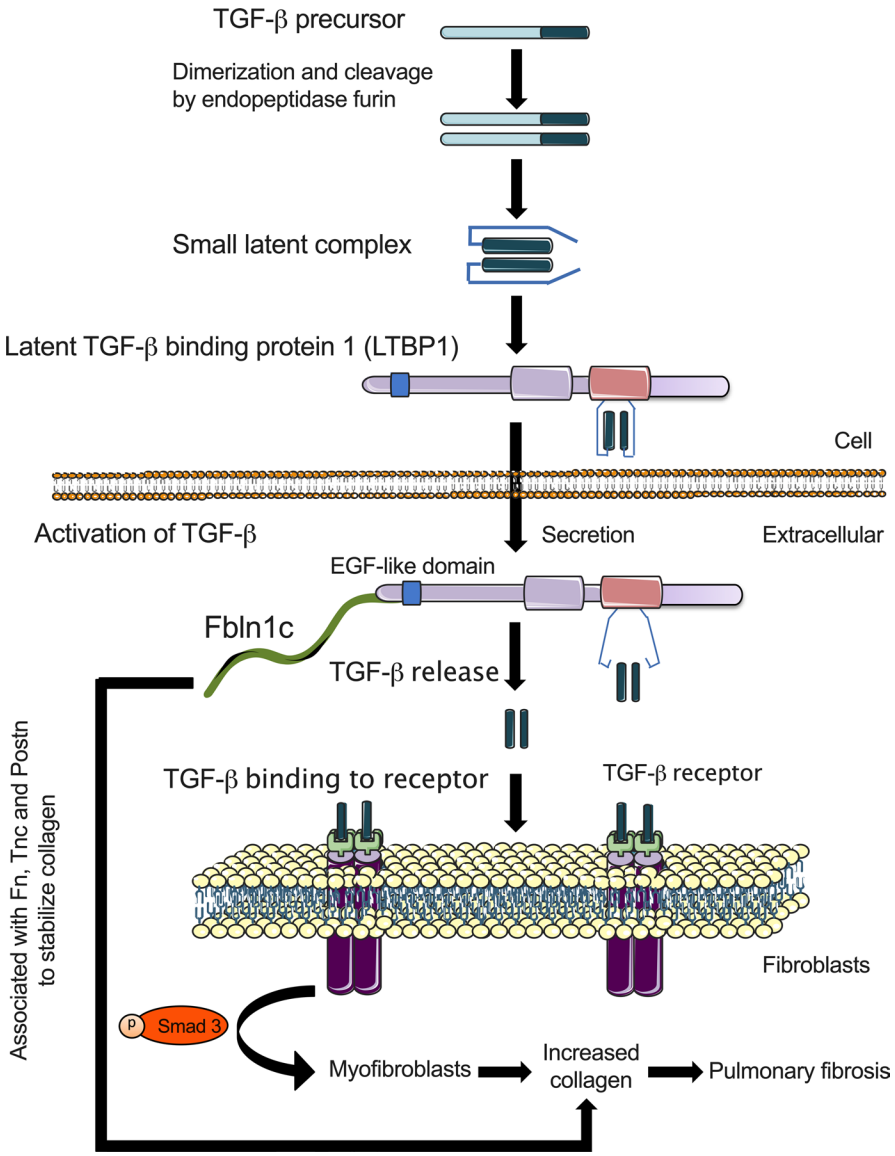

Figure 7. Proposed role of Fbln1c in pulmonary fibrosis: Fbln1c binds to LTBP1 to activate TGF-β and induce myofibroblast proliferation and collagen production. TGF-β precursors dimerize and are cleaved by the endopeptidase furin to form small latent complexes. LTBP1 binds to small latent complexes, and the entire combination is secreted into the extracellular space. Fbln1c protein binds to LTBP1 likely via EGF-like domains on both, causing the release of activated TGF-β. Fbln1c-induced, activated TGF-β binds to its receptor on the surface of fibroblasts to stimulate the development and proliferation of myofibroblasts through the activity of p-Smad3, causing increased collagen production and pulmonary fibrosis. Fbln1c also associates with Fn, Tnc, and Postn to stabilize the resulting collagen structure.

TGF-β is the archetypal profibrotic cytokine that is increased in IPF lungs (18) and promotes cell proliferation and remodeling processes. It is initially synthesized in a precursor form, dimerizes, and is cleaved by the protease furin (41). This results in the release of a small latent complex, which attaches to LTBP1 (41). Anchoring of this complex to the ECM occurs through interactions of ECM proteins with the EGF-like repeat domains on the N-terminus of the LTBP1 protein (42). From the anchored complex, activated TGF-β is released via several mechanisms, which induce downstream signaling pathways (43). Fbln1c contains EGF-like binding regions (16), which in itself indicates a potential role in TGF-β activation. We showed that Fbln1 and LTBP1 colocalized in lungs from patients with IPF. Interestingly, monkey Fbln1c was reported to interact with heparin-binding EGF-like modules (44). Other studies show that Fbln5 binds to the N-terminal EGF-like domain of LTBP2 (45). We showed that Fbln1c binds with LTBP1 and regulates TGF-β activation. TGF-β signaling via Smad effectors is well known to be involved in cell growth and proliferation and ECM deposition in fibroblasts (43). Previous

studies demonstrated reduced Smad3 mRNA and protein levels in the lungs of mice with bleomycin-induced pulmonary fibrosis (46). We corroborated these decreases in *Smad3* mRNA expression but in contrast found increased p-Smad3 protein levels in WT mouse lungs after bleomycin challenge and fibroblasts after TGF-β stimulation. However, the altered p-Smad3 levels did not occur in the absence of *Fbln1c*. This demonstrates roles for Fbln1c in controlling TGF-β activation and signaling pathways that lead to pulmonary fibrosis.

We found that lung fibroblasts from WT mice incubated with BALF from *Fbln1c*$^{-/-}$ mice for 6 hours reduce p-Smad3 and collagen proteins compared with those cells received in BALF from WT mice. Longer incubations (24 and 48 hours) with BALF from *Fbln1c*$^{-/-}$ mice resulted in fibroblasts detached from plates. The exact reason remains unclear, although the fibroblasts' detachment may be due to decreased collagen. Many studies have shown that collagen is essential to assist fibroblasts' attachment (47). LTBP1 is secreted into the airway fluid; however, the lack of active TGF-β in the BALF of *Fbln1c*$^{-/-}$ mice reduced the collagen levels in fibroblasts. This further supports our findings that Fbln1c regulates TGF-β activation.

Integrins are cell membrane receptors that facilitate ECM protein binding and adhesion. They are also involved in TGF-β activation; Henderson et al. showed that inhibition of the expression of the α_v subunit reduced TGF-β levels in fibroblasts and protected against fibrosis in an experimental animal model of liver fibrosis (47, 48). This study also suggested that $\alpha_v\beta_1$ integrin is a major regulator of TGF-β activation. There are several therapeutic compounds that target the α_v integrin that are currently in clinical trials to reduce fibrosis (48). Previous studies showed that Fbln1c might be mediated through $\alpha_v\beta_1$ integrin signaling; however, the relationship between Fbln1c and integrins in lung fibrosis remains unknown.

ECM proteins are deposited in excess in many pulmonary diseases, and Fbln1, in particular Fbln1c, is involved in regulating remodeling and fibrosis in lungs (1, 20). We have shown that genetic inhibition of Fbln1c in mice substantially reduced pulmonary remodeling and fibrosis in cigarette smoke–induced COPD and house dust mite–induced asthma (1, 20). Our previous studies also showed that specific inhibition of Fbln1c gene expression with siRNA also similarly reduced remodeling features. Thus, targeting the Fbln1c gene, for example with antisense oligonucleotides, may be a therapeutic option to reduce fibrosis in lungs. We show that Fbln1c regulates fibrosis by binding with LTBP1 to control TGF-β activation. Inhibiting Fbln1c binding to LTBP1 binding is another potential therapeutic option to reduce active TGF-β and lung fibrosis.

We showed that TGF-β–induced conversion of fibroblasts to myofibroblasts is substantially reduced in the absence of Fbln1c. Fibroblasts/myofibroblasts are the major cellular source of collagen (49). These cells have altered autophagic pathways in patients with IPF (50), produce more Fbln1 (18), and are important in maintaining a pathological profibrotic phenotype, particularly in a collagen-rich environment (51).

We previously showed that Fbln1, but not specifically Fbln1c, protein levels were increased in the serum/plasma and lung tissue of patients with IPF (18). Fbln1, like other ECM proteins, is constantly being produced and degraded. This is partly because of the activity of specific proteases, such as MMP13 (52). Peptide products resulting from ECM degradation are not necessarily inert and may have immunomodulatory effects. Peptides from ECM degradation induce the proliferation, migration, and MMP production and ECM deposition of airway smooth muscle (ASM) cells and myofibroblasts (53, 54). Protein fragments generated by MMP activity are increased in the serum of patients with IPF compared with healthy controls and are associated with disease progression (55). Other studies showed that Fbln1c peptides increase the attachment of ASM cells and fibroblasts (19). Also, Fbln1c peptide stimulates Fbln1 deposition in fibroblasts from patients with IPF and augments the production of Fn and perlecan (19). Thus, the increase in Fbln1 and Fbln1c may provide substrates for MMPs to generate peptide fragments that contribute to the development of remodeling and disease in IPF.

Considering previous and our new data together, Fbln1c associates with Fn, Tnc, and Postn to stabilize the resulting collagen structure. It also induces increased MMP activity that drives the production of ECM fragments, further stimulating fibroblast activity and perpetuating fibrosis. Collectively these events promote the deposition of ECM and stabilize exaggerated ECM formation around the airways and in lung tissues in IPF. We propose (Figure 7) that excess Fbln1c is induced during remodeling events and promotes the development of fibrosis. TGF-β precursors dimerize and are cleaved by the endopeptidase furin to form small latent complexes (41). LTBP1 binds to these complexes and the entire combination is secreted into the extracellular space (42). Fbln1c protein binds to LTBP1 via EGF-like domains, causing the release of activated TGF-β. It also regulates fibroblasts' activation and the TGF-β signaling pathway to induce myofibroblast development and collagen production. This study provides our fundamental knowledge of fibrosis and further increases understanding of mechanism of TGF-β activation. Thus, Fbln1c may be a novel therapeutic target for suppressing fibrosis in IPF and potentially other fibrotic diseases.

Methods

Human lung tissue. Lung tissue for Fbln1c immunohistochemistry staining (Figure 1A) was obtained from patients with IPF (n = 7). All patients with IPF had end-stage disease and underwent lung transplantation (Table 1). The non-IPF control group (n = 8) consisted of 4 donor lungs that were not used in transplantation and lung tissues from 4 subjects with normal lung function (FEV_1 > 80% and FEV_1/FVC ratio > 0.7) who had lung tissue removed for thoracic malignancies. Human tissues for colocalization immunohistochemical staining (Figure 6) were procured from nontransplantable donors and patients with IPF undergoing lung transplantation or lung resection.

Immunohistochemistry and remodeling. Human and mouse lung longitudinal sections on slides were incubated with citrate buffer (10 mM sodium citrate, 0.05% Tween-20, pH 6) for antigen retrieval after deparaffinization. Lung sections were blocked with casein (MilliporeSigma) at room temperature for 1 hour. Slides were incubated with monoclonal anti-Fbln1c antibody (mAB5D12, 1:50), which was produced as previously described (16), and Fbln1 (1:50, Abcam), Col1a1 (1:100, Abcam), Tnc (1:50, Santa Cruz Biotechnology), Fn (1:100, MilliporeSigma), and Postn (1:100, Abcam) antibodies, at 4°C overnight, followed by antirabbit secondary antibody (R&D Systems) at room temperature for 1 hour. Diaminobenzidine (DAKO) was applied and hematoxylin was used to counterstain the sections. Lung remodeling analyses were assessed as previously described (1, 18).

Mice and experimental model. Female 6- to 8-week-old WT C57BL/6J or *Fbln1c*$^{-/-}$ mice were housed in specific pathogen–free conditions. *Fbln1c*$^{-/-}$ mice were generated as previously described (1). Experimental pulmonary fibrosis was induced by administration of a single dose of bleomycin sulfate (0.05 U/mouse, MP Biomedical) as described previously (21–23). Controls received an equal volume of sterile PBS. Tissues were collected 7, 14, 21, and 28 days after bleomycin challenge.

Lung remodeling. Formalin-fixed, paraffin-embedded mouse lung sections were deparaffinized with xylene and a graded ethanol series (56). Collagen was stained with Verhoeff-Van Gieson stain (Australian Biostain). Fbln1, Fbln1c, Fn, Tnc, and Postn were stained by immunofluorescence or immunohistochemistry. Photomicrographs were taken with an Axio Imager M2 microscope (Zeiss) and images evaluated with ImageJ (version 1.47, NIH) as previously described (23, 57, 58). Briefly, at least 6 airways per mouse were selected while blinded to condition from 4–8 animals in each group, and images were captured with an Aperio AT2 (Leica Biosystems). Mouse small airways were defined as those having the Pbm less than 1 mm (59). The Pbm, the inner collagen area (Ai) and the outer collagen area (Ao) were manually measured using ImageJ. The collagen area (Wct) was calculated (Wct = Ao – Ai) and normalized to the Pbm. For quantification in whole lungs, Fbln1c area was normalized to total area as previously described (18).

Hydroxyproline. Hydroxyproline content in mouse whole lung tissues were assessed as a measure of lung collagen levels. Content was measured colorimetrically as previously described (1, 60, 61).

Soluble collagen assay. Soluble collagen was determined using Sircol Collagen Assay kits (S1000, Biocolor) according to the manufacturer's instructions with modifications as previously described (1).

Protein extraction and immunoblotting. Mouse lung tissues were snap-frozen and thawed before being homogenized in radioimmunoprecipitation assay buffer (MilliporeSigma) supplemented with PhosSTOP phosphatase inhibitor and complete protease inhibitor cocktails (Roche) and centrifuged (8000 *g*, 10 minutes, 4°C) as previously described (58, 62). Proteins were collected for immunoblot assay or ELISA. Protein concentrations were determined using a BCA protein assay kit (Pierce Biotechnology).

Proteins were separated by SDS-PAGE using Mini-PROTEAN TGX Stain-Free gels (Bio-Rad) and transferred to polyvinylidene fluoride membranes (MilliporeSigma) (63). Proteins of interest were detected using Fbln1 (1:2000, ab175204, Abcam), the Fbln1c antibody described above, Col1a1 (1:5000, ab34170, Abcam), Tnc (1:500, sc20932, Santa Cruz Biotechnology), Fn (1:4000, F3648, MilliporeSigma), Postn (1:4000, ab14041, Abcam), LTBP1 (1:1000, abs504, MilliporeSigma), p-Smad3 (1:2000, ab52903, Abcam), vinculin (1:10,000, ab129002, Abcam), and β-actin (1:10,000, ab8227, Abcam) antibodies at 4°C overnight. Blots were incubated with antimouse (ab97023, Abcam) or antirabbit horseradish peroxidase–conjugated secondary antibody (HAF008, R&D systems) at room temperature for 2 hours. Images of immunoblots were captured with a ChemiDoc MP System (Bio-Rad). Some blots were cut based on the protein molecular weight. ImageJ was used for densitometry analysis as described previously (1, 64).

Immunofluorescence. Mouse and human lungs were formalin fixed and paraffin embedded (1, 56, 65, 66). Sections were cut to 4-μm thickness. Slides were deparaffinized and incubated with Tris buffer (10 mM Tris base, 0.5% Tween 20, pH 9) at 100°C for antigen retrieval and blocked with casein (Milli-

poreSigma) at room temperature for 2 hours. Slides were stained with the Fbln1c antibody (1:20) that was conjugated with FITC using a kit (ab102884, Abcam) at 4°C overnight. Nuclei were counterstained with Hoechst (1:200, MilliporeSigma) at room temperature for 5 minutes (65). Images were taken using an Axio Imager M2 microscope.

Mouse primary fibroblasts were fixed with 3% paraformaldehyde in PBS (pH 7.4) at room temperature for 10 minutes, permeabilized with 0.2% Triton X-100, blocked with casein at room temperature for 1 hour, and incubated with anti–mouse β-actin antibody (1:1000, ab8227, Abcam) at room temperature for 1 hour. After 3 PBS-Tween washes, cells were incubated with FITC-conjugated antimouse secondary antibody (1:1000, ab6717, Abcam) at room temperature for 1 hour. Cells were incubated with a Cy3-conjugated anti–mouse α-SMA antibody (1:200, c6198, MilliporeSigma) at room temperature for 2 hours, and nuclei were counterstained with Hoechst. Per section, 10 random images were visualized using an Axio Imager M2 microscope and analyzed using imaging software (Zen, Zeiss). The percentage of myofibroblasts was calculated as the percentage of α-SMA–positive cells in the total cell number (β-actin–positive cells).

Human lung sections were deparaffinized and incubated with citrate for antigen retrieval at 100°C for 15 minutes. Slides were incubated overnight with anti-Fbln1 (1:50, ab211536, Abcam) in PBS with 1% BSA at 4°C overnight, followed by antimouse Alexa Fluor 647–conjugated secondary antibody (1:100, A-31571, Thermo Fisher Scientific) at room temperature for 2 hours. After slides were washed with PBS, they were incubated with anti-LTBP1 (1:100, ab78294, Abcam) at room temperature for 2 hours, followed by antirabbit Alexa Fluor 555–conjugated secondary antibody (1:100, A-31572 Thermo Fisher Scientific). Nuclei were counterstained with DAPI (10236276001, MilliporeSigma). Fluorescence signals were examined using a Leica TCS SP8 confocal microscope (Leica Microsystems).

ELISA. Cytokines in lung tissues were assessed by ELISA as previously described (58, 67). The concentrations of TGF-β were determined using capture and detection antibodies (555052 and 555053, BD Pharmingen), according to the manufacturer's instructions. The levels of target proteins in lungs were normalized to total lung protein.

Immunoprecipitation. Fbln1c proteins were immunoprecipitated from lung homogenates from WT and *Fbln1c*$^{-/-}$ mice using a Dynabead protein A immunoprecipitation kit (10006D, Life Technologies) according to the manufacturer's instructions. Briefly, Fbln1c antibody (10 μg) was added to lung homogenates and incubated with rotation at 4°C overnight. Dynabeads (1.5 mg), superparamagnetic particles that have specific affinity to bind to antibody, were added into the protein and antibody complex and incubated with rotation at 4°C for 1 hour. The bead–antibody and protein complex were separated from the solution by magnet. Nonbinding proteins were washed off 3 times with PBS, and target proteins were collected by adding elution buffer (from kit) and Laemmli sample buffer (1610747, Bio-Rad) containing 2-mercaptoethanol (1610710, Bio-Rad) and heated at 90°C for 10 minutes. SDS-PAGE was used to detect the target Fbln1c protein and its binding partners.

RNA extraction and qRT-PCR. Total RNA was extracted using TRIzol (Invitrogen) and reverse-transcribed using Bioscript (Bioline) and random hexamer primers (Invitrogen). Quantitative real-time PCR (qRT-PCR) was performed using SYBR reagents and a Viia 7 real-time PCR system (Life Technologies). Primers are listed in Table 2. mRNA levels were normalized to those of the housekeeping gene hypoxanthine-guanine phosphoribosyltransferase and expressed as relative abundance in the control group (67, 68).

SHG microscopy. Formalin-fixed, paraffin-embedded mouse lung sections were cut to 10-μm thickness. Sections were deparaffinized with xylene and a graded ethanol series, then dehydrated and coverslipped for SHG using a Leica SP5 multiphoton confocal system with an excitation wavelength of 810 nm throughout. F_{SHG} and B_{SHG} signals were obtained, and image analysis was performed using Fiji with images imported from LAS AF software as previously described (24, 69). In brief, a quarter-wave plate (CVI Laser Optics) was used to produce circularly polarized light to detect maximum collagen content. The incident laser power was adjusted to the same level (25 mW) throughout the experiment, and SHG signals were detected with a 405/10-nm band-pass filter. Then, 10 random pictures without large airways and blood vessels were selected. The pixel area (the number of pixels with intensity above threshold) and total signal intensity (total intensity for all pixels with intensity above threshold) were determined and the average values calculated for every image in the stack. The process was repeated for both F_{SHG}- and B_{SHG}-propagated signals. The ratio of F_{SHG}/B_{SHG} signal was then calculated for area measurements.

Lung function. Mice were anesthetized (50 μL/10 g, intraperitoneally) with a mix of xylazine (2 mg/mL, Troy Laboratories) and ketamine (40 mg/mL, Parnell). Mice were tracheotomized and a cannula was inserted into the trachea. Animals were ventilated with a tidal volume of 8 mL/kg at a rate of 450

Table 2. Primers for qRT-PCR

Gene	Forward primer 5′ to 3′	Reverse primer 5′ to 3′
Col1a1	CTTCACCTACAGCACCCTTGTG	TGACTGTCTTGCCCCAAGTTC
Fbln1c	AGAACTATCGCCGCTCCGCA	CCACCGCTGGCACTTGGATG
Fbln1d	GCTATGAGGACGGCATGACT	GGAAACTACGCCTCCCAACA
Fn	TGTGGTTGCCTTGCACGAT	GCTATCCACTGGGCAGTAAAGC
HPRT	AGGCCAGACTTTGTTGGATTTGAA	CAACTTGCGCTCATCTTAGGCTTT
MMP1	GTCTTCTGGCACACGCTTTT	GGGCAGCAACAATAAACAA
MMP3	ACATGGAGACTTTGTCCCTTTTG	TTGGCTGAGTGGTAGAGTCCC
MMP8	GATTCAGAAGAAACGTGGACTCAA	CATCAAGGCACCAGGATCAGT
MMP12	GCTTGAGTTTTGATGGTGTCAC	GAAGTAATGTTGGTGGCTGGGA
MMP13	CCTTCTGGTCTTCTGGCACAC	GGCTGGGTCACACTTCTCTGG
Postn	CACGGCATGGTTATTCCTTCA	TCAGGACACGGTCAATGACAT
Smad2	AATACGGTAGATCAGTGGGACA	CAGTTTTCGATTGCCTTGAGC
Smad3	GTTCTCCAAACCTCTCCCCG	TGTGAGGCGTGGAATGTCTC
Smad4	AGCCGTCCTTACCCACTGAA	GGTGGTAGTGCTGTTATGATGGT
Tgfb	CCCGAAGCGGACTACTATGCTA	GGTAACGCCAGGAATTGTTGCTAT
TIMP1	ATCTGGCATCCTCTTGTTGCT	CTCGTTGATTTCTGGGGAACC
Tnc	TCCCCAAGAGAATTTACAGCTACAG	AGATTCATAGACCAGGAGGTATCCA

breaths/min, with increased airway pressure from 2–30 cmH_2O into mouse lungs to measure baseline lung function parameters, including tissue damping, tissue elastance, and lung compliance using invasive plethysmography with the forced oscillation technique and Flexivent apparatus (Scireq) as previously described (1, 56, 58, 70).

Lung fibroblast isolation and culture. Lungs were excised from 6-week-old WT or *Fbln1c*$^{-/-}$ mice, and primary fibroblasts were isolated as described previously (71, 72). The cells were cultured in Dulbecco's modified Eagle medium (DMEM, D5671, MilliporeSigma) containing 10% fetal bovine serum (Bovogen), 25 mmol HEPES buffer, 100 U/mL penicillin, and 100 μg/mL streptomycin (37°C, 5% CO_2) and used from passages 3–7. Primary fibroblasts were seeded at 5000 cells/cm^2 and incubated overnight to allow cells to form a monolayer. Fibroblasts were stimulated with recombinant TGF-β protein (5 ng/mL, R&D Systems) supplemented with 0.5% FCS in DMEM or with medium only (control) for 48 hours. Cell lysates were collected for RNA and protein extraction, and myofibroblasts were analyzed using immunofluorescence.

Lung fibroblasts were isolated from WT mice and cultured in 6-well plates with BALF (20 L each mouse, 6 mice per group, 120 L in total in 1 mL DMEM with 10% FCS) from bleomycin-challenged or control WT and Fbln1c$^{-/-}$ mice for 6, 24, and 48 hours. Cell lysates were collected for protein analysis.

Statistics. Results are presented as mean ± SEM from 7–8 human samples or 6–8 mice in duplicate or triplicate experiments. Statistical significance of data between 2 groups was determined using a 2-tailed Student's *t* test and of data from more than 2 groups was analyzed using 1-way ANOVA with Bonferroni's posttest and GraphPad Prism software (version 6). Statistical differences were accepted at $P < 0.05$.

Study approval. All procedures were approved by the University of Newcastle or the University Medical Centre Groningen Human and Animal Ethics Committees. The human subjects and/or their guardians provided informed consent before participation in this study.

Author contributions

GL, AGJ, JCH, JKB, and PMH participated in the design of the study. GL performed in vivo and part of the in vitro experiments. MAC and WSA generated *Fbln1c*$^{-/-}$ mice and provided Fbln1c antibody. PMN, TJH, CLH, and BJ assisted with mouse experiments. ACH and MF assisted with immunoprecipitation experiments. GT performed SHG experiments. BGO and JKB performed human lung collections. TB performed the human colocalization experiment. DAK assisted with experimental design. NGH contributed to preparation and editing of the manuscript. All authors participated in the interpretation of data, manuscript preparation, and editing of the manuscript for intellectual content. GL, MAC, AGJ, TB, PMN, GT, ACH, TJH, MF, CLH, BJ, NGH, PAW, JCH, WSA, BGO, DAK, JKB, and PMH read and approved the final manuscript (WSA passed away before the final version was completed).

Acknowledgments

This work was supported as follows. GL was supported by Lung Foundation Australia/Lizotte Family Research Award. The NIH supported WSA and MAC. AGJ was supported by Lung Foundation of Australia/Boehringer Ingelheim COPD Research Fellowship. BGO and JKB were supported by National Health and Medical Research Council (NHMRC) Career Development Fellowships. JKB was supported by a University of Groningen/European Union Rosalind Franklin Fellowship. PMH received fellowships and grants from NHMRC of Australia (NHMRC 1079187) and the Brawn Foundation, Faculty of Health and Medicine, the University of Newcastle. This work is dedicated to the memory of W. Scott Argraves, who passed away during the completion of this study.

Address correspondence to: Philip M. Hansbro, Building 93, Royal prince Alfred hospital, Missenden Road, Comperdown, NSW 2050 Australia. Phone: 61.2.9565.6248; Email: Philip.Hansbro@uts.edu.au.

1. Liu G, et al. Fibulin-1 regulates the pathogenesis of tissue remodeling in respiratory diseases. *JCI Insight*. 2016;1(9):e86380.
2. Ge L, et al. miR-323a-3p regulates lung fibrosis by targeting multiple profibrotic pathways. *JCI Insight*. 2016;1(20):e90301.
3. Wynn TA. Integrating mechanisms of pulmonary fibrosis. *J Exp Med*. 2011;208(7):1339–1350.
4. Adachi K, Yamauchi K, Bernaudin JF, Fouret P, Ferrans VJ, Crystal RG. Evaluation of fibronectin gene expression by in situ hybridization. Differential expression of the fibronectin gene among populations of human alveolar macrophages. *Am J Pathol*. 1988;133(2):193–203.
5. Uchida M, et al. Periostin, a matricellular protein, plays a role in the induction of chemokines in pulmonary fibrosis. *Am J Respir Cell Mol Biol*. 2012;46(5):677–686.
6. King TE, et al. A phase 3 trial of pirfenidone in patients with idiopathic pulmonary fibrosis. *N Engl J Med*. 2014;370(22):2083–2092.
7. Navaratnam V, et al. The rising incidence of idiopathic pulmonary fibrosis in the U.K. *Thorax*. 2011;66(6):462–467.
8. Raghu G, et al. An official ATS/ERS/JRS/ALAT statement: idiopathic pulmonary fibrosis: evidence-based guidelines for diagnosis and management. *Am J Respir Crit Care Med*. 2011;183(6):788–824.
9. King TE, Pardo A, Selman M. Idiopathic pulmonary fibrosis. *Lancet*. 2011;378(9807):1949–1961.
10. Ponticos M, et al. Pivotal role of connective tissue growth factor in lung fibrosis: MAPK-dependent transcriptional activation of type I collagen. *Arthritis Rheum*. 2009;60(7):2142–2155.
11. Crouch E. Pathobiology of pulmonary fibrosis. *Am J Physiol*. 1990;259(4 Pt 1):L159–L184.
12. Collard HR, King TE, Bartelson BB, Vourlekis JS, Schwarz MI, Brown KK. Changes in clinical and physiologic variables predict survival in idiopathic pulmonary fibrosis. *Am J Respir Crit Care Med*. 2003;168(5):538–542.
13. Lawson WE, et al. Genetic mutations in surfactant protein C are a rare cause of sporadic cases of IPF. *Thorax*. 2004;59(11):977–980.
14. Pardo A, Selman M. Lung fibroblasts, aging, and idiopathic pulmonary fibrosis. *Ann Am Thorac Soc*. 2016;13 Suppl 5:S417–S421.
15. Richeldi L, et al. Efficacy and safety of nintedanib in idiopathic pulmonary fibrosis. *N Engl J Med*. 2014;370(22):2071–2082.
16. Argraves WS, Tran H, Burgess WH, Dickerson K. Fibulin is an extracellular matrix and plasma glycoprotein with repeated domain structure. *J Cell Biol*. 1990;111(6 Pt 2):3155–3164.
17. Roark EF, Keene DR, Haudenschild CC, Godyna S, Little CD, Argraves WS. The association of human fibulin-1 with elastic fibers: an immunohistological, ultrastructural, and RNA study. *J Histochem Cytochem*. 1995;43(4):401–411.
18. Jaffar J, et al. Fibulin-1 predicts disease progression in patients with idiopathic pulmonary fibrosis. *Chest*. 2014;146(4):1055–1063.
19. Ge Q, et al. Fibulin1C peptide induces cell attachment and extracellular matrix deposition in lung fibroblasts. *Sci Rep*. 2015;5:9496.
20. Liu G, et al. Airway remodelling and inflammation in asthma are dependent on the extracellular matrix protein fibulin-1c. *J Pathol*. 2017;243(4):510–523.
21. Hattori N, et al. Bleomycin-induced pulmonary fibrosis in fibrinogen-null mice. *J Clin Invest*. 2000;106(11):1341–1350.
22. Xiao J, et al. miR-29 inhibits bleomycin-induced pulmonary fibrosis in mice. *Mol Ther*. 2012;20(6):1251–1260.
23. Gold MJ, et al. Mucosal production of uric acid by airway epithelial cells contributes to particulate matter-induced allergic sensitization. *Mucosal Immunol*. 2016;9(3):809–820.
24. Tjin G, Xu P, Kable SH, Kable EP, Burgess JK. Quantification of collagen I in airway tissues using second harmonic generation. *J Biomed Opt*. 2014;19(3):36005.
25. Tjin G, et al. Lysyl oxidases regulate fibrillar collagen remodelling in idiopathic pulmonary fibrosis. *Dis Model Mech*. 2017;10(11):1301–1312.
26. Moore BB, Hogaboam CM. Murine models of pulmonary fibrosis. *Am J Physiol Lung Cell Mol Physiol*. 2008;294(2):L152–L160.
27. de Vega S, Iwamoto T, Yamada Y. Fibulins: multiple roles in matrix structures and tissue functions. *Cell Mol Life Sci*. 2009;66(11-12):1890–1902.
28. Yamashita CM, et al. Matrix metalloproteinase 3 is a mediator of pulmonary fibrosis. *Am J Pathol*. 2011;179(4):1733–1745.
29. Craig VJ, et al. Mononuclear phagocytes and airway epithelial cells: novel sources of matrix metalloproteinase-8 (MMP-8) in patients with idiopathic pulmonary fibrosis. *PLoS ONE*. 2014;9(5):e97485.
30. Dancer RC, Wood AM, Thickett DR. Metalloproteinases in idiopathic pulmonary fibrosis. *Eur Respir J*. 2011;38(6):1461–1467.
31. Vanoirbeek JA, et al. Noninvasive and invasive pulmonary function in mouse models of obstructive and restrictive respiratory diseases. *Am J Respir Cell Mol Biol*. 2010;42(1):96–104.
32. Fritz DK, et al. A mouse model of airway disease: oncostatin M-induced pulmonary eosinophilia, goblet cell hyperplasia, and airway hyperresponsiveness are STAT6 dependent, and interstitial pulmonary fibrosis is STAT6 independent. *J Immunol*. 2011;186(2):1107–1118.

33. Booth AJ, et al. Acellular normal and fibrotic human lung matrices as a culture system for in vitro investigation. *Am J Respir Crit Care Med*. 2012;186(9):866–876.
34. Clarke DL, Carruthers AM, Mustelin T, Murray LA. Matrix regulation of idiopathic pulmonary fibrosis: the role of enzymes. *Fibrogenesis Tissue Repair*. 2013;6(1):20.
35. Estany S, et al. Lung fibrotic tenascin-C upregulation is associated with other extracellular matrix proteins and induced by TGFβ1. *BMC Pulm Med*. 2014;14:120.
36. Norris RA, et al. Periostin regulates collagen fibrillogenesis and the biomechanical properties of connective tissues. *J Cell Biochem*. 2007;101(3):695–711.
37. Bensadoun ES, Burke AK, Hogg JC, Roberts CR. Proteoglycan deposition in pulmonary fibrosis. *Am J Respir Crit Care Med*. 1996;154(6 Pt 1):1819–1828.
38. Blaauboer ME, et al. Extracellular matrix proteins: a positive feedback loop in lung fibrosis? *Matrix Biol*. 2014;34:170–178.
39. Burgess JK, et al. Reduction of tumstatin in asthmatic airways contributes to angiogenesis, inflammation, and hyperresponsiveness. *Am J Respir Crit Care Med*. 2010;181(2):106–115.
40. Conickx G, et al. MicroRNA profiling reveals a role for microRNA-218-5p in the pathogenesis of chronic obstructive pulmonary disease. *Am J Respir Crit Care Med*. 2017;195(1):43–56.
41. Fortunel NO, Hatzfeld A, Hatzfeld JA. Transforming growth factor-beta: pleiotropic role in the regulation of hematopoiesis. *Blood*. 2000;96(6):2022–2036.
42. Kanzaki T, et al. TGF-beta 1 binding protein: a component of the large latent complex of TGF-beta 1 with multiple repeat sequences. *Cell*. 1990;61(6):1051–1061.
43. ten Dijke P, Arthur HM. Extracellular control of TGFbeta signalling in vascular development and disease. *Nat Rev Mol Cell Biol*. 2007;8(11):857–869.
44. Brooke JS, Cha JH, Eidels L. Latent transforming growth factor beta-binding protein-3 and fibulin-1C interact with the extracellular domain of the heparin-binding EGF-like growth factor precursor. *BMC Cell Biol*. 2002;3:2.
45. Hirai M, Horiguchi M, Ohbayashi T, Kita T, Chien KR, Nakamura T. Latent TGF-beta-binding protein 2 binds to DANCE/fibulin-5 and regulates elastic fiber assembly. *EMBO J*. 2007;26(14):3283–3295.
46. Zhao Y, Geverd DA. Regulation of Smad3 expression in bleomycin-induced pulmonary fibrosis: a negative feedback loop of TGF-beta signaling. *Biochem Biophys Res Commun*. 2002;294(2):319–323.
47. Jokinen J, et al. Integrin-mediated cell adhesion to type I collagen fibrils. *J Biol Chem*. 2004;279(30):31956–31963.
48. Henderson NC, et al. Targeting of αv integrin identifies a core molecular pathway that regulates fibrosis in several organs. *Nat Med*. 2013;19(12):1617–1624.
49. Phan SH. The myofibroblast in pulmonary fibrosis. *Chest*. 2002;122(6 Suppl):286S–289S.
50. Ricci A, et al. Decreased expression of autophagic beclin 1 protein in idiopathic pulmonary fibrosis fibroblasts. *J Cell Physiol*. 2013;228(7):1516–1524.
51. Nho RS, Hergert P. IPF fibroblasts are desensitized to type I collagen matrix-induced cell death by suppressing low autophagy via aberrant Akt/mTOR kinases. *PLoS ONE*. 2014;9(4):e94616.
52. Wang Q, et al. Extracellular calumenin suppresses ERK1/2 signaling and cell migration by protecting fibulin-1 from MMP-13-mediated proteolysis. *Oncogene*. 2015;34(8):1006–1018.
53. López B, González A, Díez J. Role of matrix metalloproteinases in hypertension-associated cardiac fibrosis. *Curr Opin Nephrol Hypertens*. 2004;13(2):197–204.
54. Harkness LM, Weckmann M, Kopp M, Becker T, Ashton AW, Burgess JK. Tumstatin regulates the angiogenic and inflammatory potential of airway smooth muscle extracellular matrix. *J Cell Mol Med*. 2017;21(12):3288–3297.
55. Jenkins RG, et al. Longitudinal change in collagen degradation biomarkers in idiopathic pulmonary fibrosis: an analysis from the prospective, multicentre PROFILE study. *Lancet Respir Med*. 2015;3(6):462–472.
56. Thorburn AN, Foster PS, Gibson PG, Hansbro PM. Components of Streptococcus pneumoniae suppress allergic airways disease and NKT cells by inducing regulatory T cells. *J Immunol*. 2012;188(9):4611–4620.
57. Hansbro PM, et al. Importance of mast cell Prss31/transmembrane tryptase/tryptase-γ in lung function and experimental chronic obstructive pulmonary disease and colitis. *J Biol Chem*. 2014;289(26):18214–18227.
58. Haw TJ, et al. A pathogenic role for tumor necrosis factor-related apoptosis-inducing ligand in chronic obstructive pulmonary disease. *Mucosal Immunol*. 2016;9(4):859–872.
59. Palmans E, Kips JC, Pauwels RA. Prolonged allergen exposure induces structural airway changes in sensitized rats. *Am J Respir Crit Care Med*. 2000;161(2 Pt 1):627–635.
60. Woessner JF. The determination of hydroxyproline in tissue and protein samples containing small proportions of this imino acid. *Arch Biochem Biophys*. 1961;93:440–447.
61. Jarnicki AG, et al. The inhibitor of semicarbazide-sensitive amine oxidase, PXS-4728A, ameliorates key features of chronic obstructive pulmonary disease in a mouse model. *Br J Pharmacol*. 2016;173(22):3161–3175.
62. Kim RY, et al. MicroRNA-21 drives severe, steroid-insensitive experimental asthma by amplifying phosphoinositide 3-kinase-mediated suppression of histone deacetylase 2. *J Allergy Clin Immunol*. 2017;139(2):519–532.
63. Kim RY, et al. Role for NLRP3 inflammasome-mediated, IL-1β-dependent responses in severe, steroid-resistant asthma. *Am J Respir Crit Care Med*. 2017;196(3):283–297.
64. Hsu AC, et al. Targeting PI3K-p110α suppresses influenza virus infection in chronic obstructive pulmonary disease. *Am J Respir Crit Care Med*. 2015;191(9):1012–1023.
65. Kaiko GE, et al. Chlamydia muridarum infection subverts dendritic cell function to promote Th2 immunity and airways hyperreactivity. *J Immunol*. 2008;180(4):2225–2232.
66. Liu G, et al. Platelet activating factor receptor regulates colitis-induced pulmonary inflammation through the NLRP3 inflammasome. *Mucosal Immunol*. 2019;12(4):862–873.
67. Essilfie AT, et al. Macrolide therapy suppresses key features of experimental steroid-sensitive and steroid-insensitive asthma. *Thorax*. 2015;70(5):458–467.
68. Asquith KL, et al. Interleukin-13 promotes susceptibility to chlamydial infection of the respiratory and genital tracts. *PLoS Pat-*

hog. 2011;7(5):e1001339.
69. Kottmann RM, et al. Second harmonic generation microscopy reveals altered collagen microstructure in usual interstitial pneumonia versus healthy lung. *Respir Res*. 2015;16:61.
70. Preston JA, et al. Inhibition of allergic airways disease by immunomodulatory therapy with whole killed Streptococcus pneumoniae. *Vaccine*. 2007;25(48):8154–8162.
71. Hinz B, Celetta G, Tomasek JJ, Gabbiani G, Chaponnier C. Alpha-smooth muscle actin expression upregulates fibroblast contractile activity. *Mol Biol Cell*. 2001;12(9):2730–2741.
72. Seluanov A, Vaidya A, Gorbunova V. Establishing primary adult fibroblast cultures from rodents. *J Vis Exp*. 2010(44):e2033.